

# MCPDepth: Omnidirectional Depth Estimation via Stereo Matching from Multi-Cylindrical Panoramas

Feng Qiao<sup>1</sup>, Zhexiao Xiong<sup>1</sup>, Xinge Zhu<sup>2</sup>, Yuexin Ma<sup>3</sup>, Qiumeng He<sup>4</sup>, Nathan Jacobs<sup>1</sup>

<sup>1</sup>Washington University in St. Louis <sup>2</sup>The Chinese University of Hong Kong

<sup>3</sup>ShanghaiTech University <sup>4</sup>University of California, Los Angeles

## Abstract

We introduce *Multi-Cylindrical Panoramic Depth Estimation (MCPDepth)*, a two-stage framework for omnidirectional depth estimation via stereo matching between multiple cylindrical panoramas. MCPDepth uses cylindrical panoramas for initial stereo matching and then fuses the resulting depth maps across views. A circular attention module is employed to overcome the distortion along the vertical axis. MCPDepth exclusively utilizes standard network components, simplifying deployment to embedded devices and outperforming previous methods that require custom kernels. We theoretically and experimentally compare spherical and cylindrical projections for stereo matching, highlighting the advantages of the cylindrical projection. MCPDepth achieves state-of-the-art performance with an 18.8% reduction in mean absolute error (MAE) for depth on the outdoor synthetic dataset Deep360 and a 19.9% reduction on the indoor real-scene dataset 3D60.

## 1. Introduction

Depth estimation is a fundamental challenge in geometric computer vision. Omnidirectional depth estimation has recently gained tremendous progress with the advent of convolutional neural networks and has been widely applied in robot perception. Various methods have been proposed for both monocular [15, 44] and binocular [19, 20, 46] settings. Some utilize regular convolution for spherical projection [15, 44, 46], while others do not simplify the spherical epipolar constraint [19]. Additionally, some methods employ customized convolutions, such as deformable convolution [41], EquiConvs [9], and spherical convolution [20], which pose deployment challenges [38, 53] on robot platforms. Furthermore, depth estimation from one or two views is unreliable and error-prone.

Several works have explored the multi-view setting to overcome these challenges, such as SweepNet [51] and OmniMVS [50], utilizing four fish-eye cameras. However,

these methods struggle with effective feature extraction due to distortion and large field-of-view (FoV) as they rely on regular convolutions. In addition, the blind spots in fish-eye cameras contribute to discontinuities in the spherical cost volume.

MODE [20] introduces a two-stage framework of omnidirectional depth estimation from multi-view spherical panoramas and proposes the Deep360 dataset. MODE adopts spherical convolutions [7] to address the distortion problem in spherical panoramas, encountering deployment challenges [38]. MODE also employs Cassini projection [48] for stereo matching to simplify the epipolar constraint. Cassini projection, the transverse aspect of the equirectangular projection (ERP), is widely used in map projection. However, compared to cylindrical projection [1], Cassini projection has greater distortion, which increases the closer it gets to the poles.

We adopt the two-stage structure from MODE [20] but use multi-view panoramas in cylindrical projection. This projection reduces distortion, avoids customized convolutions, and maintains a simple epipolar constraint. Fig. 1 illustrates the differences between Cassini and cylindrical projections for stereo matching and their respective performances. We also propose a circular attention module to better capture panorama features with a 360° vertical FoV and overcome vertical axis distortion.

Our contributions can be summarized as follows:

- We present the first omnidirectional depth estimation framework via stereo matching between multiple cylindrical panoramas.
- We theoretically and experimentally compare spherical and cylindrical projections for stereo matching, summarizing the advantages of cylindrical projection.
- We propose a circular attention module to address vertical axis distortion in cylindrical panoramas and enhance the receptive fields of convolutional neural networks (CNNs).
- Our approach achieves state-of-the-art performance on the outdoor synthetic dataset Deep360 and the indoor real-scene dataset 3D60.

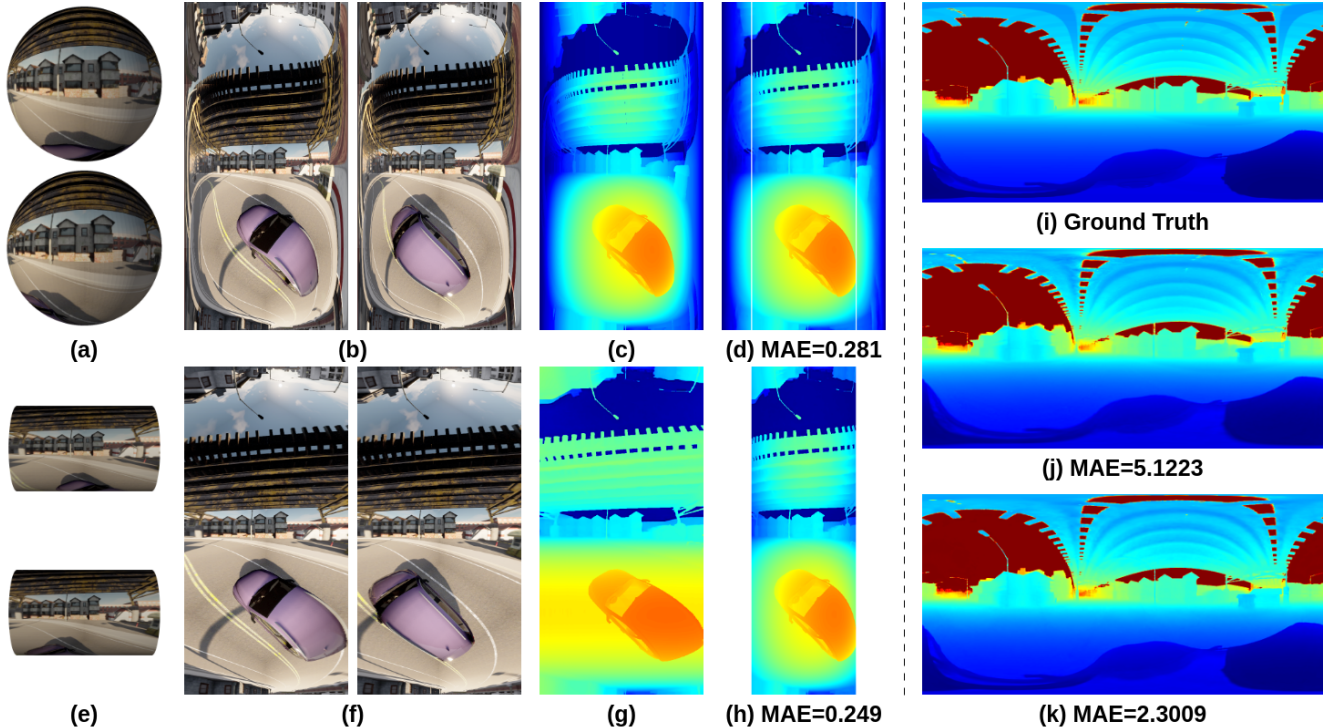


Figure 1. Comparison between MODE and our method. The left part of the figure compares the performance of MODE and our method on the stereo matching task. The first and second columns display the results from MODE and our method, respectively. (a) and (b) show spheres and spherical stereo panoramas. (c) presents disparity ground truth and (d) the estimated disparity map from MODE. (e) and (f) depict cylinders and cylindrical stereo panoramas. (g) shows the estimated disparity map from our method, and (h) displays the converted disparity map in Cassini projection from (g), we evaluate the corresponding center area in (d). On the right part, (i), (j), and (k) represent the ground truth of the depth map, the depth map from MODE, and the depth map from our method, respectively. Our method outperforms MODE in both stereo matching and depth estimation tasks.

## 2. Related Work

### 2.1. Deep Learning-based Stereo Matching

Early methods used deep neural networks to compute matching costs, like MCCNN [58], which trains a CNN for initial patch matching costs. Recently, end-to-end neural networks have dominated the stereo matching methods. Works such as [11, 22, 23, 28, 30, 40, 55] only use 2D convolutions. Mayer *et al.* [28] propose the first end-to-end disparity estimation network, DispNet, and its correlation version, DispNetC. Pang *et al.* [30] introduce a two-stage framework named CRL with multi-scale residual learning. GwcNet [11] proposes the group-wise correlation volume to improve the expressiveness of the cost volume and performance in ambiguous regions.

AANet [55] adopts a novel aggregation algorithm using sparse points and multi-scale interaction. Another series of works [3, 16] use 3D convolutions, which have great potential in regularizing or filtering the cost volume. GCNet [16] firstly uses 3D encoder-decoder architecture to regularize a 4D concatenation volume. PSMNet [3] proposes a stacked

hourglass 3D CNN in conjunction with intermediate supervision to regularize the concatenation volume.

Recently, iterative methods [18, 25, 43, 54] have shown impressive results. RAFTStereo [25] proposes to recurrently update the disparity field using local cost values retrieved from the all-pairs correlations. IGEV-Stereo [54] introduces a geometry encoding volume to encode non-local geometry and context information.

Significant advancements have also been made in multi-view stereo (MVS) [4, 10, 56, 57]. Note that these methods are designed for perspective cameras with normal FoV.

In this work, we base our experiments on the cost volume-based method PSMNet and the iterative method IGEV-Stereo.

### 2.2. Omnidirectional Depth Estimation

Omnidirectional depth estimation has developed tremendously with neural networks. Zioulis *et al.* present a learning-based monocular depth estimation method in [61], trained directly on omnidirectional content in the ERP domain and later propose CoordNet [62] with spherical dis-

parity model. BiFuse [44] uses both equirectangular and cubemap projections for depth estimation. A more effective fusion framework for ERP and cubemap projection is proposed in Unifuse [15]. Cheng *et al.* [5] introduce a depth sensing system by combining an OmniCamera with a regular depth sensor. 360SD-Net [46] is the first end-to-end trainable network for stereo depth estimation using spherical panoramas. CSDNet [19] focuses on the left-right stereo and uses Mesh CNNs [14] to overcome the spherical distortion. SweepNet [51] and OmniMVS [50] use multi-view fish-eye images for omnidirectional depth maps. However, most of these methods are based on spherical projection and extract spherical features with regular convolutions and none of them discuss the properties of cylindrical projection.

Cheng *et al.* [5] propose a spherical feature transform layer to reduce the difficulty of feature learning. MODE [20] adopts spherical convolution from Spherenet [7], but the customized CUDA implementation poses deployment challenges on robotic computing platforms [38].

Jun *et al.* [37] employed cylindrical panoramas for stereo matching, but without CNNs or analysis of cylindrical projection properties, and the panoramas were stitched from 12 perspective images. MCPDepth is the first to explore the advantages of cylindrical projection over spherical projection for stereo matching and to use cylindrical panoramas for omnidirectional depth estimation.

### 2.3. Self-Attention Module

Attention mechanisms are first introduced by [2] for the encoder-decoder in a neural sequence-to-sequence model. It is designed to capture the correspondence of tokens between two sequences. Self-attention, designed for single contexts, can encode long-range interactions. Recently, self-attention has been widely applied in computer vision and achieves state-of-the-art performance [6, 13, 29, 31, 32, 39, 42, 47, 59].

In stereo matching, CREStereo [18] first adopts the self-attention module from LoFTR [39]. Zhao *et al.* [60] propose a multi-stage and multi-scale channel-attention transformer to preserve high-frequency information. GOAT [26] uses self-cross attention to capture more representative and distinguishable features. However, these methods are not designed for stereo matching of panoramas with a 360° FoV.

Global self-attention in image processing is computationally expensive due to the need to calculate the relationship between every pixel and every other pixel. This limits its practical usage across all layers in a full-attention model. It is shown in [12, 35] that self-attention layers alone could be stacked to form a fully attentional model by restricting the receptive field of self-attention to a local square region.

Inspired by Axial-DeepLab [45], we propose circular attention to capture the 360° features. We apply circular attention only along the vertical axis of feature maps, which significantly reduces the training resources.

## 3. Method

### 3.1. Framework

Given  $m$  360° cameras, where  $m \geq 3$ , we have a set of  $n = C_2^m = \frac{m!}{2!(m-2)!}$  pairs of rectified panoramas  $\{(I_L^i, I_R^i)\}_{i=1}^n$  with their extrinsic parameters. Our goal is to estimate the omnidirectional depth map  $d$  for the left panorama in the first pair  $I_L^1$ . The MCPDepth framework, shown in Fig. 2, includes two stages. In the stereo matching stage,  $n$  pairs of rectified cylindrical panoramas (Fig. 2 (a)) are fed into the stereo matching network. The number of pairs ( $n$ ) and cameras ( $m$ ) varies on different datasets:  $n = 6, m = 4$  for Deep360, and  $n = 3, m = 3$  for 3D60. The resulting disparity and confidence maps (Fig. 2 (b)) are reprojected into the Cassini domain with a 180° horizontal FoV. The disparity maps are then converted to depth maps. The depth and confidence maps are aligned with the view of  $I_L^1$  using extrinsic parameters as shown in Fig. 2 (c). Black areas indicate invisible and occluded regions.

We generally follow MODE’s depth fusion stage structure. Specifically, multi-view depth maps, along with their corresponding confidence maps and reference panoramas, are inputted into two separate 2D encoder blocks. The fused depth map is then processed through a single decoder block, incorporating skip connections between the encoder and decoder blocks at each scale. The final depth map is in the Cassini domain but can be converted to the ERP domain. More details are available in the supplementary material.

### 3.2. Stereo Matching

We use the circular attention module between feature extraction and cost volume with a structure similar to PSM-Net [3]. The circular attention module augments the extracted features to capture features from a 360° FoV and overcome vertical axis distortion. These augmented features are then shifted and concatenated to build the cost volume. The disparity map is regressed through the 3D stacked hourglass network. During training, we use the L1 loss to train the network. The confidence maps are used to measure the reliability of the disparity estimation and are widely used in stereo matching tasks [34]. The confidence map is obtained during inference. Specifically, considering the disparity is obtained through a probability-weighted sum over all disparity hypotheses, we compute the corresponding confidence value by taking a probability sum over the three nearest disparity hypotheses.

**Cylindrical Projection** Fig. 3 highlights the differences between spherical projection and cylindrical projection for



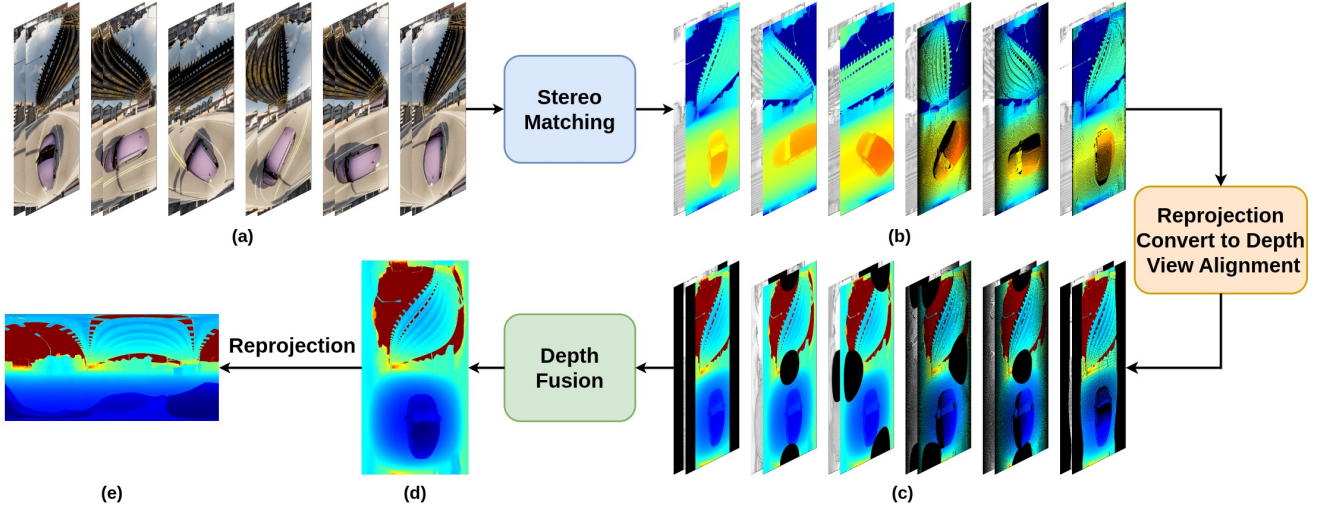


Figure 2. Framework of MCPDepth. (a) represents 6 pairs of cylindrical panoramas, (b) shows the disparity and confidence maps, and (c) shows the depth and confidence maps. (d) and (e) illustrate the depth map in Cassini and spherical projection.

stereo matching. Cylindrical projection maintains the linear epipolar constraint.

Eq. (1) illustrates the conversion between spherical and cylindrical coordinate systems and the Cartesian coordinate system. In spherical coordinates,  $\rho$  is the Euclidean distance from the origin  $O$  to point  $P$ ;  $\phi$  is the angle between line  $OP$  and the plane  $yOz$ ;  $\theta$  is the angle between line  $OP'$  and the  $z$ -axis, where  $P'$  is the projection of  $P$  on the plane of  $yOz$ . In cylindrical coordinates,  $\rho$  is the Euclidean distance from the  $x$ -axis to the point  $P$ ;  $\theta$  is the angle between line  $OP'$  and the  $z$ -axis, where  $P'$  is the projection of  $P$  on the plane of  $yOz$ .

$$\begin{cases} x = \rho \sin(\phi) \\ y = \rho \cos(\phi) \sin(\theta) \\ z = \rho \cos(\phi) \cos(\theta) \end{cases} \quad \begin{cases} x = x \\ y = \rho \sin(\theta) \\ z = \rho \cos(\theta) \end{cases} \quad (1)$$

The spherical and cylindrical panoramas in Fig. 1 (b) and (f) are generated according to Eq. (2), where  $u$  and  $v$  are pixel coordinates,  $W$  and  $H$  are panorama dimensions and  $R = H/2\pi$  is the cylinder's radius, which is the focal length in perspective images.  $u$  in the cylindrical panorama is the same as it is in the perspective images.

$$\begin{cases} u = (\phi + \frac{\pi}{2}) \cdot \frac{W}{\pi} \\ v = (\theta + \pi) \cdot \frac{H}{2\pi} \end{cases} \quad \begin{cases} u = -\frac{xR}{\rho} + \frac{W}{2} = -\frac{x}{\rho} \cdot \frac{H}{2\pi} + \frac{W}{2} \\ v = (\theta + \pi) \cdot \frac{H}{2\pi} \end{cases} \quad (2)$$

In distortion-free perspective images, an object's actual length and its pixel length along the horizontal and vertical axes is given by  $\Delta u = \frac{f_x}{z} \Delta x$ ,  $\Delta v = \frac{f_y}{z} \Delta y$ , where  $f_x, f_y$  are the focal lengths along the  $x$  and  $y$  axes, the  $z$  is the distance along the  $z$ -axis. Eq. (3) shows these relationships for both spherical and cylindrical projections.

$$\begin{cases} \Delta u = f_\phi \Delta \phi \approx \frac{f_\phi}{\rho \cos \theta} \Delta X \\ \Delta v = f_\theta \Delta \theta \approx \frac{f_\theta}{\rho} \Delta Y \end{cases} \quad \begin{cases} \Delta u = \frac{f_x}{\rho} \Delta X \\ \Delta v = f_\theta \Delta \theta \approx \frac{f_\theta}{\rho} \Delta Y \end{cases} \quad (3)$$

where all focal lengths are  $f = R = H/2\pi$  in this work. The approximation of  $\Delta X \approx \rho \cos \theta \Delta \phi$ ,  $\Delta Y \approx \rho \Delta \theta$  is under the condition that the object is not too large or far from the camera [33]. This approximation means objects in cylindrical projection appear similar regardless of their location. This shift-invariant property facilitates efficient learning by CNNs. In contrast, objects in spherical projection vary with their  $\theta$  axis position, which limits the effectiveness of regular convolutions, as shown in Fig. 3 (e).

In addition, the disparity in spherical projection is defined as angular disparity  $d$  (Fig. 3 (c)), where  $d = |\phi_l - \phi_r|$ . This concept has been previously discussed in some works [20, 21, 24, 62]. The relationship between disparity and depth is:

$$\rho_l = B \cdot \frac{\sin(\phi_r + \frac{\pi}{2})}{\sin(d)} = B \cdot \left[ \frac{\sin(\phi_l + \frac{\pi}{2})}{\tan(d)} - \cos(\phi_l + \frac{\pi}{2}) \right] \quad (4)$$

where  $B$  denotes the baseline between left and right origins. As shown in Fig. 3 (d), the cylindrical projection maintains the same disparity-depth relationship as perspective images:

$$\rho_l = \frac{B \cdot R}{|x_l - x_r|} \quad (5)$$

The benefits of cylindrical projection for stereo matching of panoramas can be summarized as (1) Compatibility with perspective images: Disparity in cylindrical panoramas is



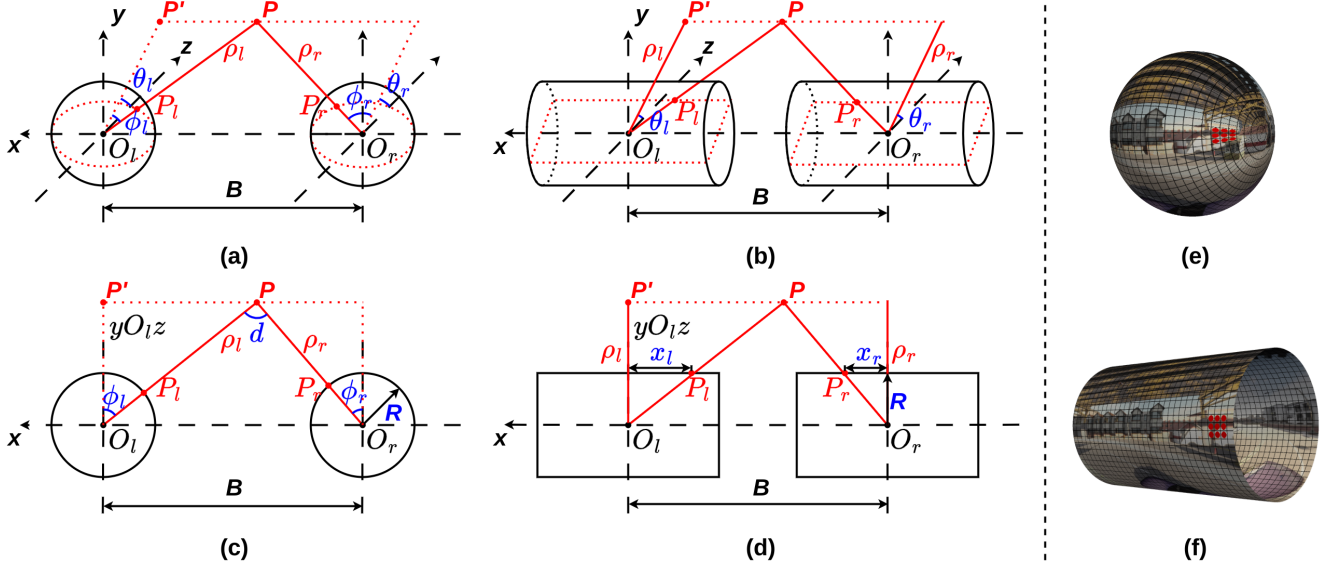


Figure 3. (a) and (b) compare the spherical and cylindrical projections for stereo matching and their respective epipolar geometries. (c) and (d) represent the schematic drawing of the epipolar plane under spherical and cylindrical projections. (e) and (f) show the different sampling patterns on the sphere and the cylinder when regular convolutions are applied to spherical and cylindrical panoramas.

defined as  $d = |x_l - x_r|$ , matching the disparity in perspective images. This allows stereo matching networks designed for perspective images to be directly applicable. (2) Reduced distortion: Spherical projection introduces distortion along both the vertical and horizontal axes, with distortion increasing near the poles. In contrast, cylindrical projection exhibits distortion solely along the vertical axis. This better shift-invariant property shown in Fig. 3 (f) enables CNNs to learn features more efficiently. (3) Simplified Deployment: Spherical panoramas require customized convolutions [7, 9, 41] to extract features. For example, spherical convolutions in MODE can't be exported to widely used ONNX [49] format for deployment, they either need CUDA Plugins for the TensorRT engine on NVIDIA platforms or customized implementation on other embedded devices. Cylindrical panoramas only use regular convolutions, making MCPDepth deployment-friendly.

**Circular Attention** To overcome vertical axis distortion and capture the circular 360° features, we introduce a circular attention module. Conventional CNNs have limited receptive fields, which is restrictive for 360° FoV panoramas. The circular attention module, placed between feature extraction and cost volume construction is flexible and can be easily integrated since it maintains the input dimension. Besides, it only calculates the relations along the vertical axis, conserving more training resources compared to global self-attention approaches. Fig. 4 (a) demonstrates our circular attention module.

In global self-attention, given an input feature map  $x \in \mathbb{R}^{h \times w \times d_{in}}$  with height  $h$ , width  $w$ , and channels  $d_{in}$ . The

output  $y_o \in \mathbb{R}^{d_{out}}$  at position  $o = (i, j)$  can be calculated as:

$$y_o = \sum_{p \in \mathcal{N}} \text{softmax}_p(q_o^T k_p) v_p \quad (6)$$

where  $\mathcal{N}$  is the whole location lattice,  $p = (a, b)$  are all possible positions. Queries  $q_o = W_Q x_o$ , keys  $k_o = W_K x_o$ , and values  $v_o = W_V x_o$  are all linear projections of the input  $x_o$ , where  $\forall o \in \mathcal{N}$ .  $W_Q, W_K \in \mathbb{R}^{d_q \times d_{in}}$ , and  $W_V \in \mathbb{R}^{d_{out} \times d_{in}}$  are all learnable weights.

However, global self-attention is extremely resource-consuming and computes ( $\mathcal{O}(h^2 w^2)$ ). Inspired by [12, 35], we restrict the receptive field of self-attention to a local region and apply only along the vertical axis. Additionally, global self-attention doesn't contain positional information, which is proven to be effective in many works [35, 36, 45, 52]. We incorporate positional information in the circular attention module. The output  $y_o$  at position  $o = (i, j)$  can be calculated as:

$$y_o = \sum_{p \in \mathcal{N}_{1 \times m}(o)} \text{softmax}_p(q_o^T k_p + q_o^T r_{p-o}^q + k_p^T r_{p-o}^k) (v_p + r_{p-o}^v) \quad (7)$$

where  $\mathcal{N}_{1 \times m}(o)$  is the local  $1 \times m$  region centered around location  $o = (i, j)$ .  $r_{p-o}^q \in \mathbb{R}^{d_q}$  is the learnable relative positional encoding for queries and the inner product  $q_o^T r_{p-o}^q$  measures the compatibility from location  $p$  to location  $o$ . Similarly, the learnable vectors  $r_{p-o}^k \in \mathbb{R}^{d_q}$  and  $r_{p-o}^v \in \mathbb{R}^{d_{out}}$  are positional encodings for keys and values. Our circular attention module reduces the computation to ( $\mathcal{O}(hwm)$ ).

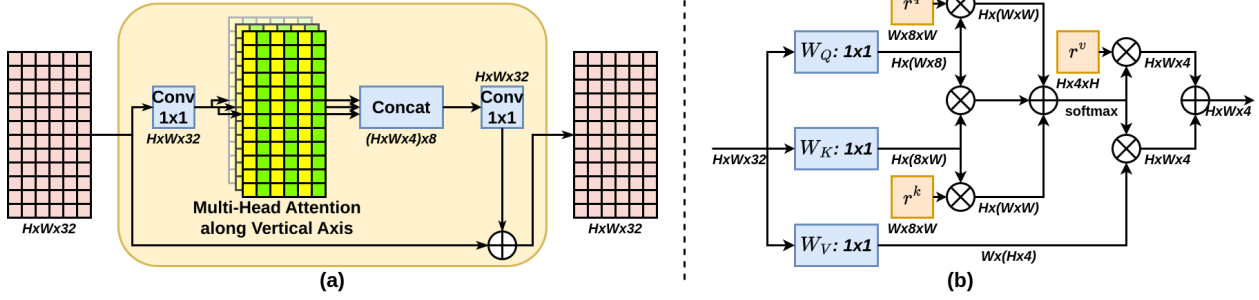


Figure 4. (a) displays the circular attention module in the stereo matching network. The number of attention heads is 8. (b) represents our attention applied along the vertical axis.  $\oplus$  denotes element-wise sum.  $\otimes$  denotes matrix multiplication. Blue boxes are  $1 \times 1$  convolution and orange boxes are relative positional encoding.

For the Deep360 dataset, the feature map size after feature extraction is  $h \times w \times d_{in} = 256 \times 128 \times 32$ . After a  $1 \times 1$  convolution is applied, the feature map is fed into a multi-head attention module, where the attention mechanism is only applied along the vertical axis. We set span  $m = 256$  to ensure it captures all features along the vertical axis. We use 8 heads, each producing  $256 \times 128 \times 4$  outputs. These are concatenated to  $256 \times 128 \times 32$ , and after another  $1 \times 1$  convolution, the feature map is added element-wise to the original. Fig. 4 (b) illustrates how one head of the circular attention module works.

## 4. Experiments

### 4.1. Datasets

We train and evaluate our framework on Deep360 [20] and 3D60 [61], which include outdoor synthetic and indoor real scenes. We evaluate both stereo matching and depth estimation tasks on them. For Deep360, 4  $360^\circ$  cameras are arranged on a horizontal plane to form a square. Panoramas from all 4 views are used to validate the performance of our framework. We use 6 pairs of stereo images for training and testing. For 3D60, 3  $360^\circ$  cameras are arranged on a vertical plane to form an equilateral right triangle. Panoramas from two of three views are used to validate the performance of our framework. The resolutions of Deep360 and 3D60 are  $H \times W = 1024 \times 512$  and  $H \times W = 512 \times 256$ , respectively.

### 4.2. Evaluation Metrics

For a fair comparison, we follow MODE [20] and evaluate stereo matching performance using MAE (mean absolute error), RMSE (root mean square error), Px1,3,5 (percentage of outliers with pixel error  $> 1, 3, 5$ ), D1 [30] (percentage of outliers with pixel error  $> 3$  and  $> 5\%$ ). We evaluate depth estimation performance using MAE, RMSE, AbsRel (absolute relative error), SqRel (square relative error), SILog [8] (scale-invariant logarithmic error),  $\delta_1, 2, 3$  [17] (accuracy with threshold that  $\max(\frac{\hat{y}}{y^*}, \frac{y^*}{\hat{y}}) <$

$1.25, 1.25^2, 1.25^3$ ).

### 4.3. Implementation Details

We use the nearest-neighbor interpolation along the horizontal axis to generate cylindrical disparity ground truth from spherical angular disparity and bi-linear interpolation to generate cylindrical panoramas from spherical ones.

In the stereo matching stage, cylindrical panoramas have a  $360^\circ$  vertical FoV and a horizontal FoV of less than  $180^\circ$ . We evaluate the central part of disparity maps in the Cassini domain with horizontal FoV  $= 2 * \arctan(\pi/2) \approx 105^\circ$  for both datasets as shown in Fig. 1 (d). This horizontal FoV can keep the size of cylindrical panoramas equal to spherical panoramas. Note that only when the horizontal FoV is greater than  $\pi/4$  can the invisible areas of a certain viewpoint be compensated by other viewpoints. In the fusion stage, we evaluate the entire omnidirectional depth map with  $360^\circ$  horizontal FoV and  $180^\circ$  vertical FoV.

### 4.4. Results

**Training on Perspective Images and Testing on Panoramas** The pre-trained models of PSMNet [3] and IGEV-Stereo [54] are trained on SceneFlow [27], which contain only perspective images. CREStereo [18], trained on mixed datasets, exhibits better generalization. The performance of stereo matching with different projections on Deep360 is shown in Tab. 1. Acquiring panoramas and their depth ground truth is difficult, the experimental results provide the potential to apply stereo-matching models trained on perspective images to cylindrical panoramas.

**Comparisons with State-of-the-Art Methods** We first evaluate our method against leading stereo matching networks such as PSMNet [3], AANet [55], and 360SD-Net [46], which is designed for  $360^\circ$  stereo. We train these models on the Deep360 training dataset from scratch and test them on the Deep360 test dataset following the default experimental settings. Tab. 2 shows that our method achieves state-of-the-art performance.

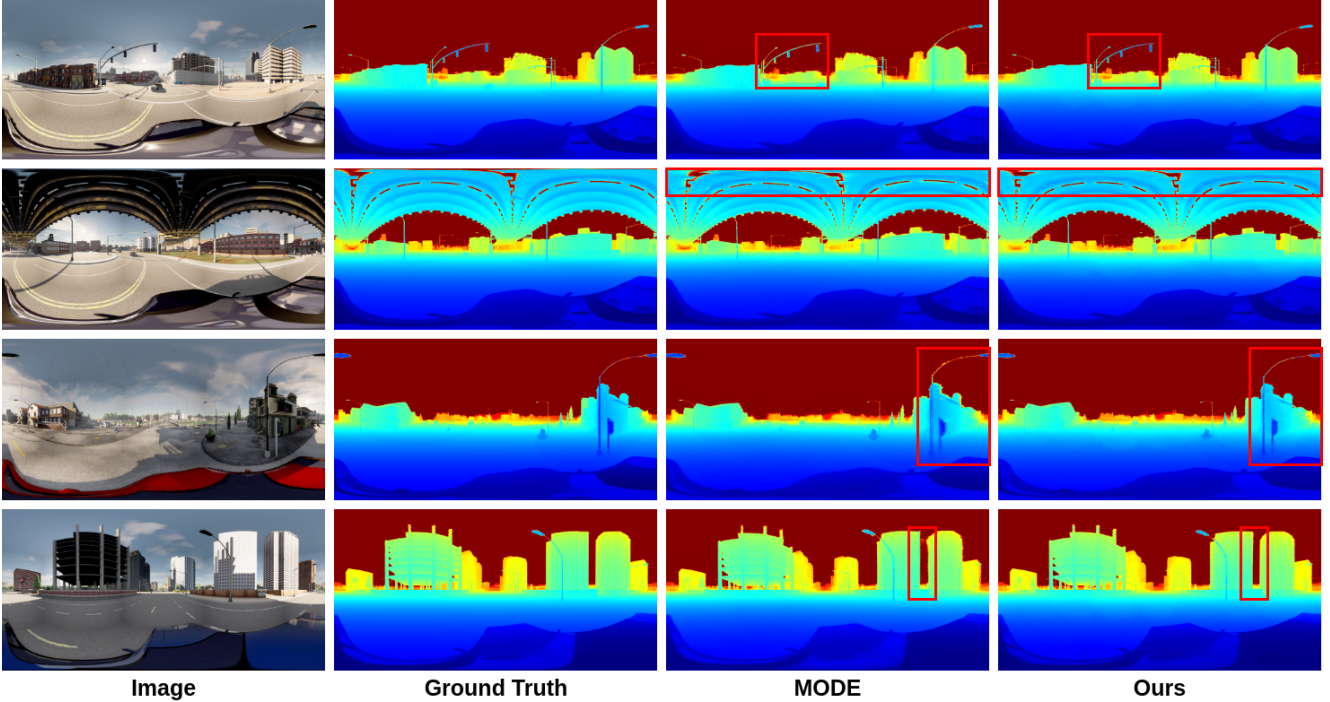


Figure 5. Depth estimation results on the Deep360 test dataset.

Table 1. Quantitative results of stereo matching models pre-trained on perspective datasets evaluated on the Deep360 test dataset under different projections.

Method	Projection	MAE	Px1 (%)	D1 (%)
PSMNet [3]	Cassini	2.7667	42.7912	12.6288
	Cylindrical	<b>2.6118</b>	<b>34.4403</b>	<b>10.8204</b>
IGEV-Stereo [54]	Cassini	6.5155	61.0948	29.7265
	Cylindrical	<b>4.0194</b>	<b>53.3429</b>	<b>22.8117</b>
CREStereo [18]	Cassini	4.6836	43.5014	18.5130
	Cylindrical	<b>2.1241</b>	<b>22.6015</b>	<b>11.2502</b>

For omnidirectional depth estimation, we compare our method with other multi-view omnidirectional depth estimation methods including UNiFuse [15], CSDNet [19], 360SD-Net [46], OmniMVS [50], and MODE [20]. We report the results from MODE. Tab. 3 shows that our method achieves an 18.8% MAE reduction on Deep360 and 19.9% on 3D60 from the best-published result.

Fig. 5 illustrates our method’s superior depth estimation on Deep360, with better handling of severe distortions, finer object details, and edges between foreground and background compared to MODE. More visual comparisons on Deep360 and 3D60 datasets are available in the supplementary material.

**Performance on Real Scenarios** We evaluate our models on real-world fisheye image pairs with a FoV of 189°. We reproject the fisheye images in spherical projection, which

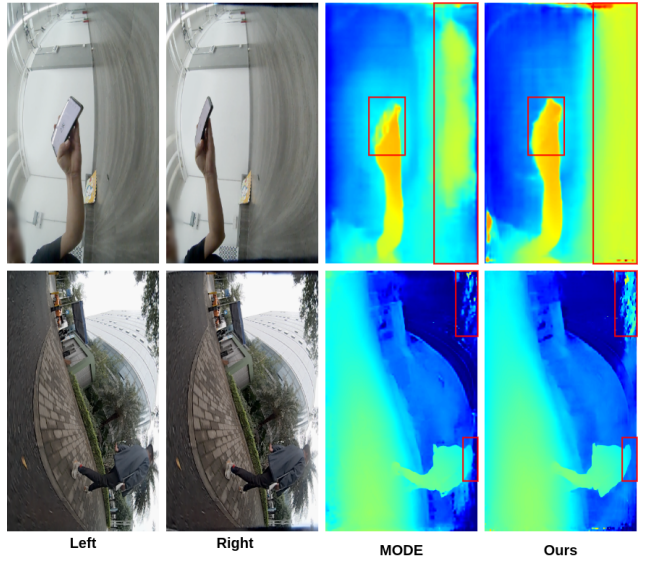


Figure 6. Depth estimation results in real-world scenarios.

have a vertical FoV of 189° and a horizontal FoV of 120°. The lens projection is equidistant, and we use OpenCV with checkerboards to calibrate the camera parameters and the relative pose of the two cameras. Fig. 6 shows the qualitative results of our models compared to MODE. For both indoor and outdoor scenes, with models trained on 3D60 and Deep360 respectively, MCPDepth demonstrates noticeable



Table 2. Quantitative results of stereo matching methods on Deep360 and 3D60 test datasets.

Dataset	Method	Projection	MAE	RMSE	Px1 (%)	Px3 (%)	Px5 (%)	D1 (%)
Deep360	AANet [55]	Cassini	0.3427	1.5703	5.2050	2.1515	1.2847	1.9817
	360SD-Net [46]	Cassini	0.5262	1.6459	3.8794	1.3389	0.8425	1.2989
	PSMNet [3]	Cassini	0.2703	1.4790	3.3556	1.1979	0.7538	1.1708
	MODE [20]	Cassini	0.2309	1.4014	2.8801	1.0488	0.6562	1.0326
	<b>Ours</b>	<b>Cylindrical</b>	<b>0.2112</b>	<b>1.3903</b>	<b>2.5713</b>	<b>1.0009</b>	<b>0.6376</b>	<b>0.9828</b>
3D60	MODE [20]	Cassini	0.2258	0.5265	2.9441	0.6482	0.2978	0.6478
	<b>Ours</b>	<b>Cylindrical</b>	<b>0.1773</b>	<b>0.4654</b>	<b>2.2298</b>	<b>0.5282</b>	<b>0.2564</b>	<b>0.5279</b>

Table 3. Quantitative results of omnidirectional depth estimation methods on Deep360 and 3D60 test datasets.

Dataset	Method	MAE(↓)	RMSE(↓)	AbsRel(↓)	SqRel(↓)	SILog(↓)	$\delta 1$ (% ↑)	$\delta 2$ (% ↑)	$\delta 3$ (% ↑)
Deep360	UniFuse [15]	3.9193	28.8475	0.0546	0.3125	0.1508	96.0269	98.2679	98.9909
	CSDNet [19]	6.6548	36.5526	0.1553	1.7898	0.2475	86.0836	95.1589	97.7562
	360SD-Net [46]	11.2643	66.5789	0.0609	0.5973	0.2438	94.8594	97.2050	98.1038
	OmniMVS [50]	8.8865	59.3043	0.1073	2.9071	0.2434	94.9611	97.5495	98.2851
	MODE [20]	3.2483	24.9391	0.0365	<b>0.0789</b>	0.1104	97.9636	99.0987	99.4683
	<b>Ours</b>	<b>2.6384</b>	<b>21.6692</b>	<b>0.0304</b>	0.1153	<b>0.1033</b>	<b>98.2557</b>	<b>99.2101</b>	<b>99.5227</b>
3D60	UniFuse [15]	0.1868	0.3947	0.0799	0.0246	0.1126	93.2860	98.4839	99.4828
	CSDNet [19]	0.2067	0.4225	0.0908	0.0241	0.1273	91.9537	98.3936	99.5109
	360SD-Net [46]	0.0762	0.2639	0.0300	0.0117	1.4578	97.6751	98.6603	99.0417
	MODE [20]	0.0713	0.2631	0.0224	0.0031	0.0512	99.1283	99.7847	99.9250
	<b>Ours</b>	<b>0.0571</b>	<b>0.1903</b>	<b>0.0199</b>	<b>0.0027</b>	<b>0.0401</b>	<b>99.3933</b>	<b>99.8506</b>	<b>99.9418</b>

improvements over MODE.

#### 4.5. Ablation Study

**Panorama Projection** Tab. 4 demonstrates that cylindrical projection outperforms spherical projection in stereo matching, even with spherical convolutions (MODE [20]). Experimental results indicate that cylindrical projection is better suited for regular convolutions and more effective for panorama stereo matching.

Table 4. Ablation study for different projections on the Deep360 test dataset. The metrics refer to disparity errors.

Method	Projection	MAE	Px1 (%)	D1 (%)
MODE [20]	Cassini	0.2309	2.8801	1.0326
PSMNet [3]	Cassini	0.2703	3.3556	1.1708
	Cylindrical	<b>0.2179</b>	<b>2.6489</b>	<b>1.0236</b>
IGEV-Stereo [54]	Cassini	0.3905	6.1733	1.8843
	Cylindrical	<b>0.3278</b>	<b>4.7958</b>	<b>1.7276</b>

**Circular Attention** Tab. 5 shows that circular attention module effectively captures 360° features and overcomes vertical axis distortion in panoramas. This module performs well across different projections and stereo-matching networks. For IGEV-Stereo [54], applying circular attention to the largest feature map (first scale) leads to significant performance gains.

## 5. Conclusion

We introduced MCPDepth, a two-stage framework for omnidirectional depth estimation via stereo matching between

Table 5. Ablation study for circular attention module on the Deep360 test dataset. "CA" denotes circular attention. The metrics refer to disparity errors.

Method	CA	Projection	MAE	Px1 (%)	D1 (%)
MODE [20]	✓	Cassini	0.2309	2.8801	1.0326
		Cassini	<b>0.2210</b>	<b>2.7537</b>	<b>0.9881</b>
PSMNet [3]	✓	Cylindrical	0.2179	2.6489	1.0236
		Cylindrical	<b>0.2112</b>	<b>2.5713</b>	<b>0.9828</b>
IGEV-Stereo [54]	✓	Cylindrical	0.3278	4.7958	1.7276
		Cylindrical	<b>0.2265</b>	<b>2.9581</b>	<b>1.1052</b>

multiple cylindrical panoramas. We conducted both theoretical and experimental comparisons between spherical and cylindrical projections for stereo matching of panoramas and analyzed the advantages of cylindrical projection. The use of cylindrical projection maintains the linear epipolar constraint, similar to the Cassini projection, and also preserves the same definition of disparity in perspective images. Furthermore, it reduces distortion and provides the potential to apply stereo-matching models trained on perspective images to cylindrical panoramas. Additionally, cylindrical projection avoids using customized kernels, making it significantly simpler for deployment to embedded devices. Apart from this, the circular attention module effectively overcomes the distortion along the vertical axis of panoramas and captures 360° features. The experimental results show that MCPDepth achieves state-of-the-art performance on the outdoor synthetic dataset Deep360 and the indoor real-scene dataset 3D60.

## References

- [1] Vertical Panoramas, also known as the vertorama — paulbourke.net. <https://paulbourke.net/panorama/vpano/>. [Accessed 29-02-2024]. 1
- [2] Dzmitry Bahdanau, Kyunghyun Cho, and Yoshua Bengio. Neural machine translation by jointly learning to align and translate. *arXiv preprint arXiv:1409.0473*, 2014. 3
- [3] Jia-Ren Chang and Yong-Sheng Chen. Pyramid stereo matching network. In *Proceedings of the IEEE conference on computer vision and pattern recognition*, pages 5410–5418, 2018. 2, 3, 6, 7, 8
- [4] Rui Chen, Songfang Han, Jing Xu, and Hao Su. Point-based multi-view stereo network. In *Proceedings of the IEEE/CVF international conference on computer vision*, pages 1538–1547, 2019. 2
- [5] Xinjing Cheng, Peng Wang, Yanqi Zhou, Chenye Guan, and Ruigang Yang. Omnidirectional depth extension networks. In *2020 IEEE International Conference on Robotics and Automation (ICRA)*, pages 589–595. IEEE, 2020. 3
- [6] Peishan Cong, Xinge Zhu, Feng Qiao, Yiming Ren, Xidong Peng, Yuenan Hou, Lan Xu, Ruigang Yang, Dinesh Manocha, and Yuexin Ma. Stcrowd: A multimodal dataset for pedestrian perception in crowded scenes. In *Proceedings of the IEEE/CVF Conference on Computer Vision and Pattern Recognition*, pages 19608–19617, 2022. 3
- [7] Benjamin Coors, Alexandru Paul Condurache, and Andreas Geiger. Spherenet: Learning spherical representations for detection and classification in omnidirectional images. In *Proceedings of the European conference on computer vision (ECCV)*, pages 518–533, 2018. 1, 3, 5
- [8] David Eigen, Christian Puhrsch, and Rob Fergus. Depth map prediction from a single image using a multi-scale deep network. *Advances in neural information processing systems*, 27, 2014. 6
- [9] Clara Fernandez-Labrador, Jose M Facil, Alejandro Perez-Yus, Cédric Demonceaux, Javier Civera, and Jose J Guerrero. Corners for layout: End-to-end layout recovery from 360 images. *IEEE Robotics and Automation Letters*, 5(2): 1255–1262, 2020. 1, 5
- [10] Xiaodong Gu, Zhiwen Fan, Siyu Zhu, Zuozhuo Dai, Feitong Tan, and Ping Tan. Cascade cost volume for high-resolution multi-view stereo and stereo matching. In *Proceedings of the IEEE/CVF conference on computer vision and pattern recognition*, pages 2495–2504, 2020. 2
- [11] Xiaoyang Guo, Kai Yang, Wukui Yang, Xiaogang Wang, and Hongsheng Li. Group-wise correlation stereo network. In *Proceedings of the IEEE/CVF conference on computer vision and pattern recognition*, pages 3273–3282, 2019. 2
- [12] Han Hu, Zheng Zhang, Zhenda Xie, and Stephen Lin. Local relation networks for image recognition. In *Proceedings of the IEEE/CVF International Conference on Computer Vision*, pages 3464–3473, 2019. 3, 5
- [13] Zilong Huang, Xinggang Wang, Lichao Huang, Chang Huang, Yunchao Wei, and Wenyu Liu. Ccnet: Criss-cross attention for semantic segmentation. In *Proceedings of the IEEE/CVF international conference on computer vision*, pages 603–612, 2019. 3
- [14] Chiyu Jiang, Jingwei Huang, Karthik Kashinath, Philip Marcus, Matthias Niessner, et al. Spherical cnns on unstructured grids. *arXiv preprint arXiv:1901.02039*, 2019. 3
- [15] Hualie Jiang, Zhe Sheng, Siyu Zhu, Zilong Dong, and Rui Huang. Unifuse: Unidirectional fusion for 360 panorama depth estimation. *IEEE Robotics and Automation Letters*, 6(2):1519–1526, 2021. 1, 3, 7, 8
- [16] Alex Kendall, Hayk Martirosyan, Saumitro Dasgupta, Peter Henry, Ryan Kennedy, Abraham Bachrach, and Adam Bry. End-to-end learning of geometry and context for deep stereo regression. In *Proceedings of the IEEE international conference on computer vision*, pages 66–75, 2017. 2
- [17] Lubor Ladicky, Jianbo Shi, and Marc Pollefeys. Pulling things out of perspective. In *Proceedings of the IEEE conference on computer vision and pattern recognition*, pages 89–96, 2014. 6
- [18] Jiankun Li, Peisen Wang, Pengfei Xiong, Tao Cai, Ziwei Yan, Lei Yang, Jiangyu Liu, Haoqiang Fan, and Shuaicheng Liu. Practical stereo matching via cascaded recurrent network with adaptive correlation. In *Proceedings of the IEEE/CVF conference on computer vision and pattern recognition*, pages 16263–16272, 2022. 2, 3, 6, 7
- [19] Ming Li, Xuejiao Hu, Jingzhao Dai, Yang Li, and Sidan Du. Omnidirectional stereo depth estimation based on spherical deep network. *Image and Vision Computing*, 114:104264, 2021. 1, 3, 7, 8
- [20] Ming Li, Xueqian Jin, Xuejiao Hu, Jingzhao Dai, Sidan Du, and Yang Li. Mode: Multi-view omnidirectional depth estimation with 360° cameras. In *European Conference on Computer Vision*, pages 197–213. Springer, 2022. 1, 3, 4, 6, 7, 8
- [21] Shigang Li. Binocular spherical stereo. *IEEE Transactions on intelligent transportation systems*, 9(4):589–600, 2008. 4
- [22] Zhaoshuo Li, Xingtong Liu, Nathan Drenkow, Andy Ding, Francis X Creighton, Russell H Taylor, and Mathias Unberath. Revisiting stereo depth estimation from a sequence-to-sequence perspective with transformers. In *Proceedings of the IEEE/CVF international conference on computer vision*, pages 6197–6206, 2021. 2
- [23] Zhengfa Liang, Yiliu Feng, Yulan Guo, Hengzhu Liu, Wei Chen, Linbo Qiao, Li Zhou, and Jianfeng Zhang. Learning for disparity estimation through feature constancy. In *Proceedings of the IEEE conference on computer vision and pattern recognition*, pages 2811–2820, 2018. 2
- [24] Kaiwen Lin and Toby P Breckon. Real-time low-cost omnidirectional stereo vision via bi-polar spherical cameras. In *Image Analysis and Recognition: 15th International Conference, ICIAR 2018, Póvoa de Varzim, Portugal, June 27–29, 2018, Proceedings 15*, pages 315–325. Springer, 2018. 4
- [25] Lahav Lipson, Zachary Teed, and Jia Deng. Raft-stereo: Multilevel recurrent field transforms for stereo matching. In *2021 International Conference on 3D Vision (3DV)*, pages 218–227. IEEE, 2021. 2
- [26] Zihua Liu, Yizhou Li, and Masatoshi Okutomi. Global occlusion-aware transformer for robust stereo matching. In *Proceedings of the IEEE/CVF Winter Conference on Applications of Computer Vision*, pages 3535–3544, 2024. 3

- [27] N. Mayer, E. Ilg, P. Häusser, P. Fischer, D. Cremers, A. Dosovitskiy, and T. Brox. A large dataset to train convolutional networks for disparity, optical flow, and scene flow estimation. In *IEEE International Conference on Computer Vision and Pattern Recognition (CVPR)*, 2016. arXiv:1512.02134. **6**
- [28] Nikolaus Mayer, Eddy Ilg, Philip Häusser, Philipp Fischer, Daniel Cremers, Alexey Dosovitskiy, and Thomas Brox. A large dataset to train convolutional networks for disparity, optical flow, and scene flow estimation. In *Proceedings of the IEEE conference on computer vision and pattern recognition*, pages 4040–4048, 2016. **2**
- [29] Ishan Misra, Rohit Girdhar, and Armand Joulin. An end-to-end transformer model for 3d object detection. In *Proceedings of the IEEE/CVF International Conference on Computer Vision (ICCV)*, pages 2906–2917, 2021. **3**
- [30] Jiahao Pang, Wenxiu Sun, Jimmy SJ Ren, Chengxi Yang, and Qiong Yan. Cascade residual learning: A two-stage convolutional neural network for stereo matching. In *Proceedings of the IEEE international conference on computer vision workshops*, pages 887–895, 2017. **2, 6**
- [31] Niki Parmar, Ashish Vaswani, Jakob Uszkoreit, Lukasz Kaiser, Noam Shazeer, Alexander Ku, and Dustin Tran. Image transformer. In *International conference on machine learning*, pages 4055–4064. PMLR, 2018. **3**
- [32] William Peebles and Saining Xie. Scalable diffusion models with transformers. In *Proceedings of the IEEE/CVF International Conference on Computer Vision (ICCV)*, pages 4195–4205, 2023. **3**
- [33] Elad Plaut, Erez Ben Yaacov, and Bat El Shlomo. 3d object detection from a single fisheye image without a single fisheye training image. In *Proceedings of the IEEE/CVF Conference on Computer Vision and Pattern Recognition*, pages 3659–3667, 2021. **4**
- [34] Matteo Poggi, Seungryong Kim, Fabio Tosi, Sunok Kim, Filippo Aleotti, Dongbo Min, Kwanghoon Sohn, and Stefano Mattoccia. On the confidence of stereo matching in a deep-learning era: a quantitative evaluation. *IEEE transactions on pattern analysis and machine intelligence*, 44(9):5293–5313, 2021. **3**
- [35] Prajit Ramachandran, Niki Parmar, Ashish Vaswani, Irwan Bello, Anselm Levskaya, and Jon Shlens. Stand-alone self-attention in vision models. *Advances in neural information processing systems*, 32, 2019. **3, 5**
- [36] Peter Shaw, Jakob Uszkoreit, and Ashish Vaswani. Self-attention with relative position representations. *arXiv preprint arXiv:1803.02155*, 2018. **5**
- [37] Jun Shimamura, Naokazu Yokoya, Haruo Takemura, and Kazumasa Yamazawa. Construction of an immersive mixed environment using an omnidirectional stereo image sensor. In *Proceedings IEEE Workshop on Omnidirectional Vision (Cat. No. PR00704)*, pages 62–69. IEEE, 2000. **3**
- [38] Yu-Chuan Su and Kristen Grauman. Learning spherical convolution for fast features from 360 imagery. *Advances in neural information processing systems*, 30, 2017. **1, 3**
- [39] Jiaming Sun, Zehong Shen, Yuang Wang, Hujun Bao, and Xiaowei Zhou. LoFTR: Detector-free local feature matching with transformers. *CVPR*, 2021. **3**
- [40] Vladimir Tankovich, Christian Hane, Yinda Zhang, Adarsh Kowdle, Sean Fanello, and Sofien Bouaziz. Hitnet: Hierarchical iterative tile refinement network for real-time stereo matching. In *Proceedings of the IEEE/CVF Conference on Computer Vision and Pattern Recognition*, pages 14362–14372, 2021. **2**
- [41] Keisuke Tateno, Nassir Navab, and Federico Tombari. Distortion-aware convolutional filters for dense prediction in panoramic images. In *Proceedings of the European Conference on Computer Vision (ECCV)*, pages 707–722, 2018. **1, 5**
- [42] Ashish Vaswani, Noam Shazeer, Niki Parmar, Jakob Uszkoreit, Llion Jones, Aidan N Gomez, Łukasz Kaiser, and Illia Polosukhin. Attention is all you need. *Advances in neural information processing systems*, 30, 2017. **3**
- [43] Fangjinhua Wang, Silvano Galliani, Christoph Vogel, and Marc Pollefeys. Itermv: Iterative probability estimation for efficient multi-view stereo. In *Proceedings of the IEEE/CVF conference on computer vision and pattern recognition*, pages 8606–8615, 2022. **2**
- [44] Fu-En Wang, Yu-Hsuan Yeh, Min Sun, Wei-Chen Chiu, and Yi-Hsuan Tsai. Bifuse: Monocular 360 depth estimation via bi-projection fusion. In *Proceedings of the IEEE/CVF Conference on Computer Vision and Pattern Recognition*, pages 462–471, 2020. **1, 3**
- [45] Huiyu Wang, Yukun Zhu, Bradley Green, Hartwig Adam, Alan Yuille, and Liang-Chieh Chen. Axial-deeplab: Stand-alone axial-attention for panoptic segmentation. In *European Conference on Computer Vision (ECCV)*, 2020. **3, 5**
- [46] Ning-Hsu Wang, Bolivar Solarte, Yi-Hsuan Tsai, Wei-Chen Chiu, and Min Sun. 360sd-net: 360 stereo depth estimation with learnable cost volume. In *2020 IEEE International Conference on Robotics and Automation (ICRA)*, pages 582–588. IEEE, 2020. **1, 3, 6, 7, 8**
- [47] Xiaolong Wang, Ross Girshick, Abhinav Gupta, and Kaiming He. Non-local neural networks. In *Proceedings of the IEEE conference on computer vision and pattern recognition*, pages 7794–7803, 2018. **3**
- [48] Wikipedia contributors. Cassini projection — Wikipedia, the free encyclopedia. [https://en.wikipedia.org/w/index.php?title=Cassini\\_projection&oldid=1184209037](https://en.wikipedia.org/w/index.php?title=Cassini_projection&oldid=1184209037), 2023. [Online; accessed 29-February-2024]. **1**
- [49] Wikipedia contributors. Open neural network exchange — Wikipedia, the free encyclopedia, 2023. [Online; accessed 6-March-2024]. **5**
- [50] Changhee Won, Jongbin Ryu, and Jongwoo Lim. Omnimvs: End-to-end learning for omnidirectional stereo matching. In *Proceedings of the IEEE/CVF International Conference on Computer Vision*, pages 8987–8996, 2019. **1, 3, 7, 8**
- [51] Changhee Won, Jongbin Ryu, and Jongwoo Lim. Sweepnet: Wide-baseline omnidirectional depth estimation. In *2019 International Conference on Robotics and Automation (ICRA)*, pages 6073–6079. IEEE, 2019. **1, 3**
- [52] Kan Wu, Houwen Peng, Minghao Chen, Jianlong Fu, and Hongyang Chao. Rethinking and improving relative position encoding for vision transformer. In *Proceedings of the*



- IEEE/CVF International Conference on Computer Vision*, pages 10033–10041, 2021. 5
- [53] Dawen Xu, Cheng Chu, Cheng Liu, Ying Wang, Huawei Li, Xiaowei Li, and Kwang-Ting Cheng. Energy-efficient accelerator design for deformable convolution networks. *arXiv preprint arXiv:2107.02547*, 2021. 1
  - [54] Gangwei Xu, Xianqi Wang, Xiaohuan Ding, and Xin Yang. Iterative geometry encoding volume for stereo matching. In *Proceedings of the IEEE/CVF Conference on Computer Vision and Pattern Recognition*, pages 21919–21928, 2023. 2, 6, 7, 8
  - [55] Haoifei Xu and Juyong Zhang. Aanet: Adaptive aggregation network for efficient stereo matching. In *Proceedings of the IEEE/CVF Conference on Computer Vision and Pattern Recognition*, pages 1959–1968, 2020. 2, 6, 8
  - [56] Jiayu Yang, Wei Mao, Jose M Alvarez, and Miaomiao Liu. Cost volume pyramid based depth inference for multi-view stereo. In *Proceedings of the IEEE/CVF Conference on Computer Vision and Pattern Recognition*, pages 4877–4886, 2020. 2
  - [57] Yao Yao, Zixin Luo, Shiwei Li, Tian Fang, and Long Quan. Mvsnet: Depth inference for unstructured multi-view stereo. In *Proceedings of the European conference on computer vision (ECCV)*, pages 767–783, 2018. 2
  - [58] Jure Zbontar and Yann LeCun. Computing the stereo matching cost with a convolutional neural network. In *Proceedings of the IEEE conference on computer vision and pattern recognition*, pages 1592–1599, 2015. 2
  - [59] Han Zhang, Ian Goodfellow, Dimitris Metaxas, and Augustus Odena. Self-attention generative adversarial networks. In *International conference on machine learning*, pages 7354–7363. PMLR, 2019. 3
  - [60] Haoliang Zhao, Huizhou Zhou, Yongjun Zhang, Jie Chen, Yitong Yang, and Yong Zhao. High-frequency stereo matching network. In *Proceedings of the IEEE/CVF Conference on Computer Vision and Pattern Recognition*, pages 1327–1336, 2023. 3
  - [61] Nikolaos Zioulis, Antonis Karakottas, Dimitrios Zarpalas, and Petros Daras. Omnidepth: Dense depth estimation for indoors spherical panoramas. In *Proceedings of the European Conference on Computer Vision (ECCV)*, pages 448–465, 2018. 2, 6, 1
  - [62] Nikolaos Zioulis, Antonis Karakottas, Dimitrios Zarpalas, Federico Alvarez, and Petros Daras. Spherical view synthesis for self-supervised 360 depth estimation. In *2019 International Conference on 3D Vision (3DV)*, pages 690–699. IEEE, 2019. 2, 4

# MCPDepth: Omnidirectional Depth Estimation via Stereo Matching from Multi-Cylindrical Panoramas

## Supplementary Material

### 6. Framework

#### 6.1. Stereo Matching

Fig. 8 shows the stereo matching network architecture with the circular attention module. Fig. 7 compares the attention heatmaps before and after circular attention. The attention module focuses primarily on the edges of objects and textured areas while paying less attention to the background and center areas of objects. This is because the disparities in the background are small, and the disparities in the center of objects are similar and contiguous.

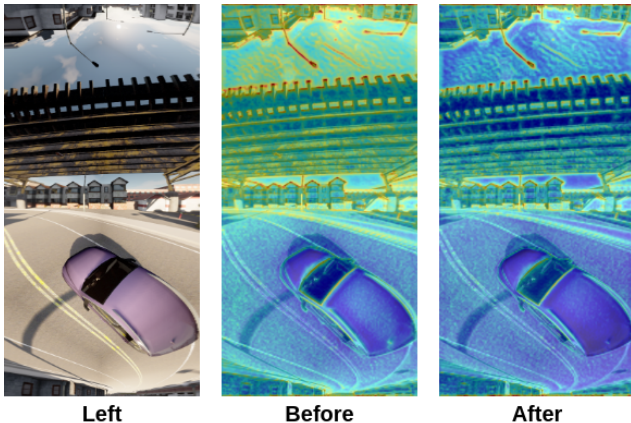


Figure 7. Comparison of heat maps before and after circular attention module.

#### 6.2. Depth Fusion

We use the depth fusion architecture from MODE [20], which takes depth maps, confidence maps, and reference panoramas. For Deep360, it uses 6 depth maps, 6 confidence maps, and 4 panoramas. For 3D60, it uses 3 of each. The Deep360 architecture is shown in Fig. 9.

### 7. Training Details

During the stereo matching stage, we use 2 NVIDIA A40 GPUs to train our models with a batch size of 4 for the Deep360 dataset. Training takes 158 hours; For 3D60, we use a single NVIDIA A6000 GPU with batch size 4, which takes 252 hours to train. The model is trained for 45 epochs with a learning rate of 0.001, followed by a decay of the learning rate to 0.0001 for an additional 10 epochs. In the depth fusion stage, we train the network for 150 epochs with a learning rate of 0.0001.

Table 6. Inference time of stereo matching model. "CA" denotes Circular Attention.

Dataset	Methods	Projection	PyTorch (ms)	ONNX (ms)
Deep360 [20]	MODE [20]	Cassini	200.62	-
	Ours w/o CA	Cylindrical	238.61	197.63
	Ours	Cylindrical	266.27	226.30
3D60 [61]	MODE [20]	Cassini	66.74	-
	Ours w/o CA	Cylindrical	66.21	46.11
	Ours	Cylindrical	69.12	51.24

### 8. Visualizations

Fig. 10 and Fig. 11 show the performance of stereo matching on Deep360 and 3D60 test datasets, our model can distinguish the foreground objects from the background, particularly in areas with severe distortion. Additionally, Fig. 12 illustrates the depth estimation performance on the 3D60 test dataset. With the help of more accurate disparity estimation, our method outperforms MODE on depth estimation performance even in areas where no ground truth is provided.

### 9. Inference Time of Stereo Matching Models

The inference time of different stereo matching models on Deep360 and 3D60 datasets are shown in Tab. 6. The models are tested in both PyTorch and ONNX formats on NVIDIA GeForce RTX 3090. The panoramas have dimensions of  $H \times W = 1024 \times 512$  on Deep360 and  $H \times W = 512 \times 256$  on 3D60 for both cylindrical and spherical projections. For Deep360, the maximum disparity is set to 272 for cylindrical projection and 192 for spherical projection, while on 3D60, the maximum disparity is set to 256 for all projections. The inference time for the circular attention module is 18.22 ms for Deep360 and 2.81 ms for 3D60.

Our stereo matching model without circular attention outperforms MODE in stereo matching performance. Additionally, it exhibits a slightly shorter inference time when handling the same maximum disparity range, as demonstrated in Tab. 6 on the 3D60 dataset compared to MODE. Furthermore, our stereo matching model, while marginally slower than MODE, provides significant advantages when exporting to the model in ONNX format. Our model in ONNX format has a much shorter inference time than MODE in PyTorch format when handling the same maximum disparity range.

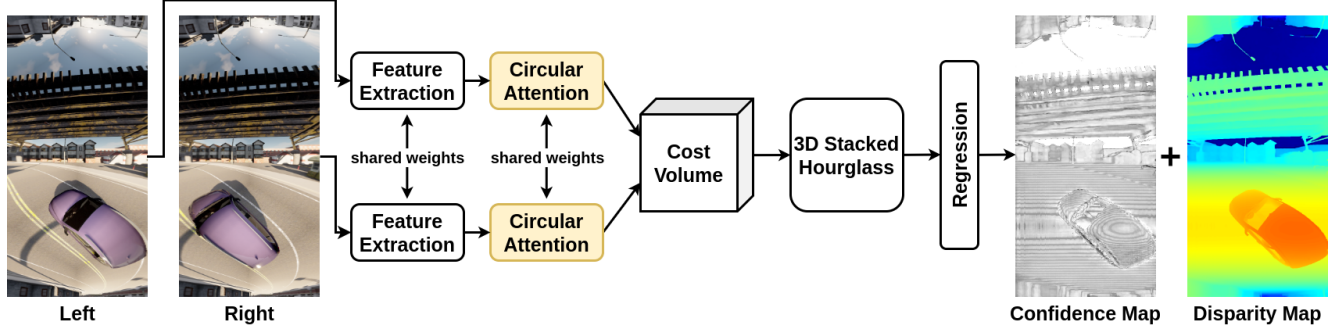


Figure 8. The architecture of the stereo matching network.

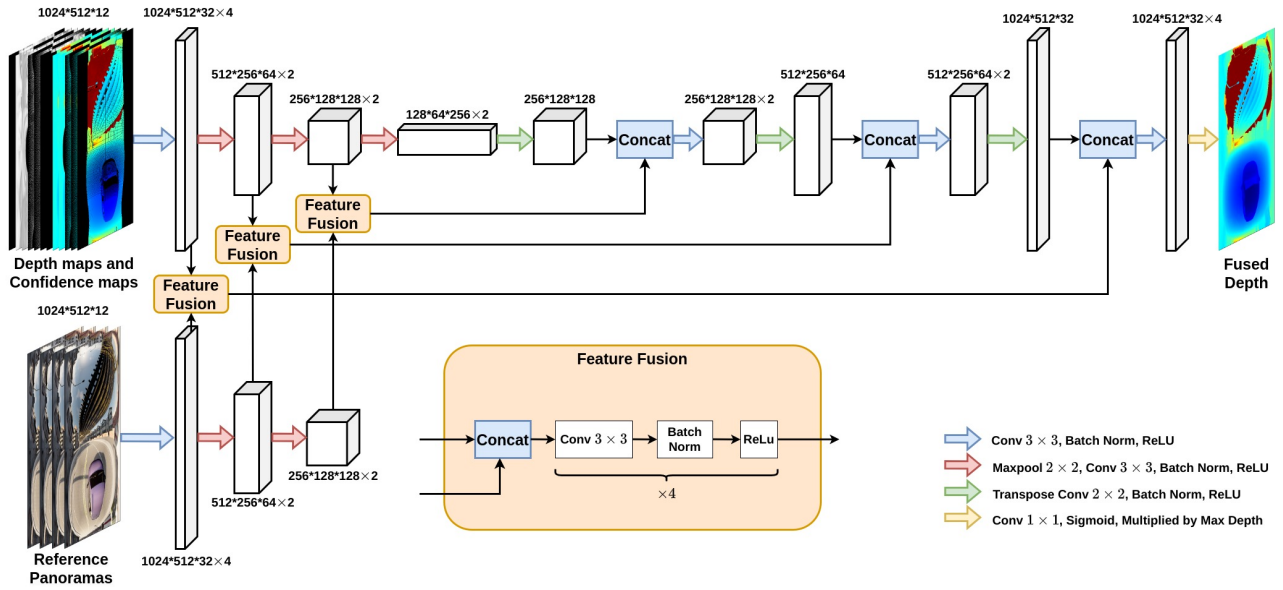


Figure 9. Depth Fusion Architecture.



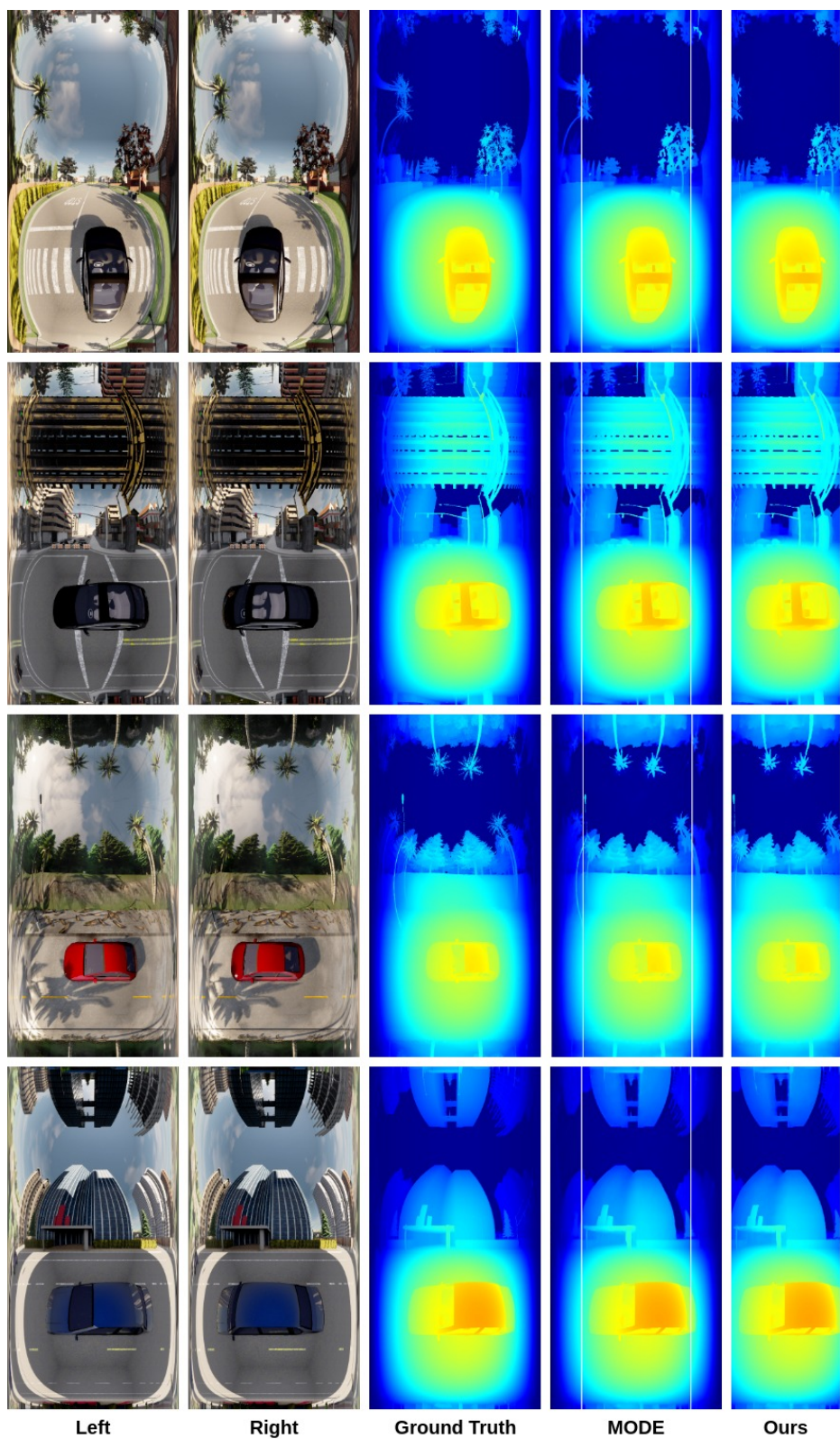


Figure 10. Disparity estimation results on the Deep360 test dataset compared to MODE.

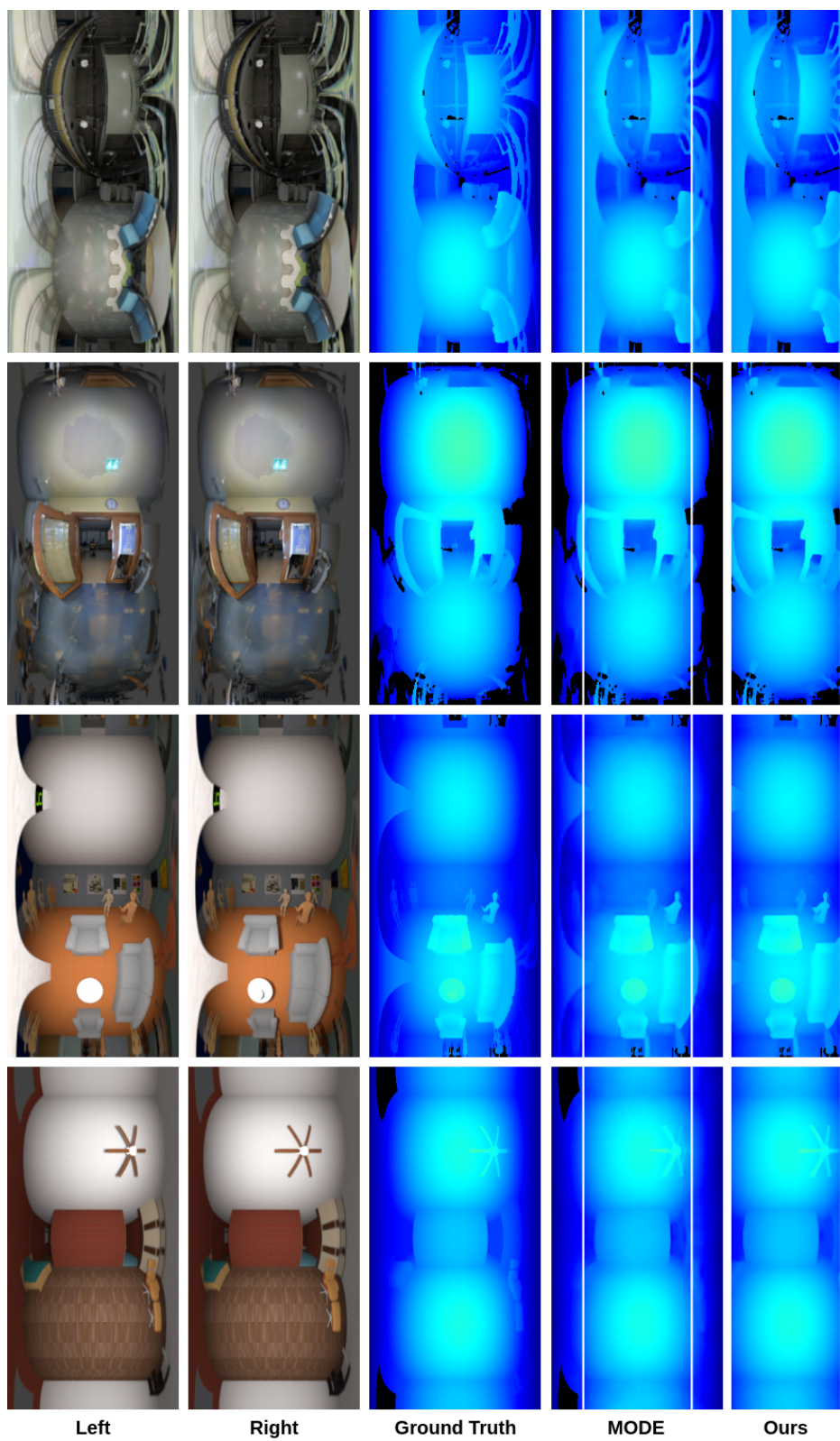


Figure 11. Disparity estimation results on the 3D60 test dataset compared to MODE.

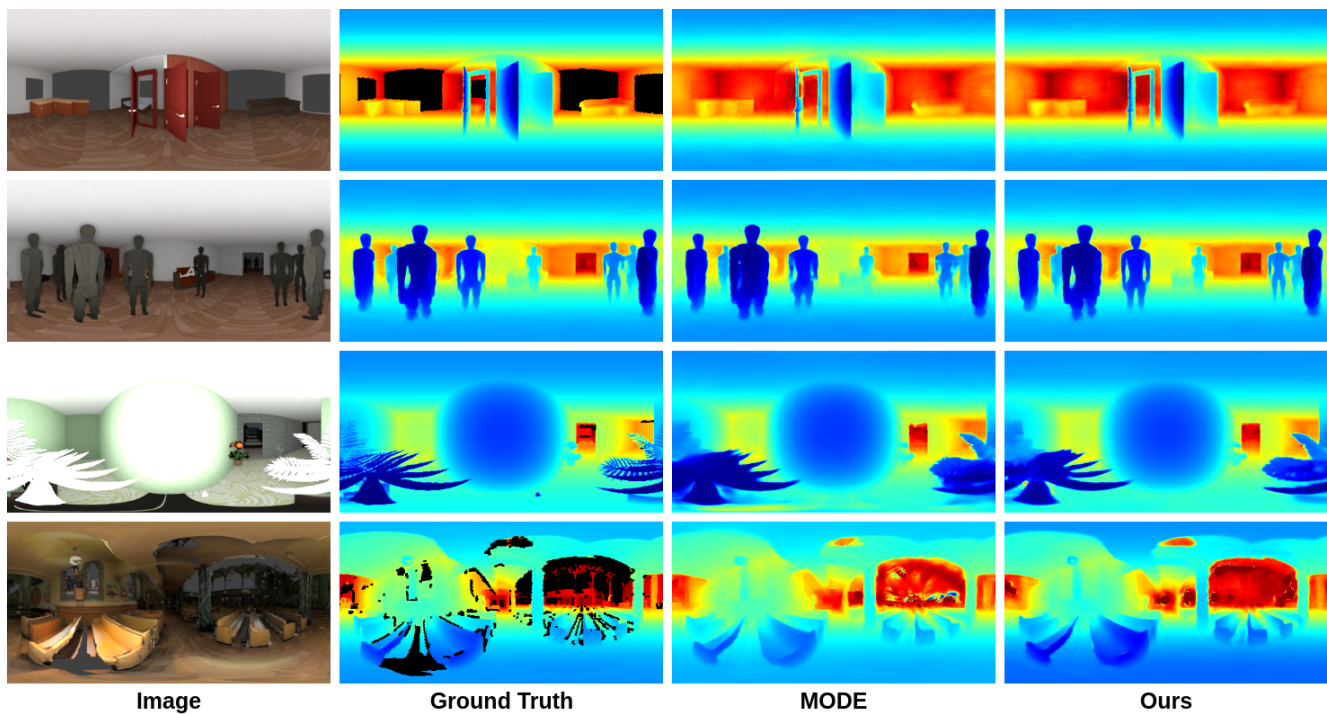


Figure 12. Qualitative comparisons of omnidirectional depth estimation methods on 3D60 compared with MODE.